

2011

A Cell Electrofusion Microfluidic Device Integrated with 3D Thin-Film Microelectrode Arrays

Ning Hu

Jun Yang


Shizhi Qian

Old Dominion University, sqian@odu.edu

Sang W. Joo

Xiaolin Zheng

Follow this and additional works at: https://digitalcommons.odu.edu/mae_fac_pubs

 Part of the [Biochemistry Commons](#), [Biophysics Commons](#), [Fluid Dynamics Commons](#), and the [Nanoscience and Nanotechnology Commons](#)

Repository Citation

Hu, Ning; Yang, Jun; Qian, Shizhi; Joo, Sang W.; and Zheng, Xiaolin, "A Cell Electrofusion Microfluidic Device Integrated with 3D Thin-Film Microelectrode Arrays" (2011). *Mechanical & Aerospace Engineering Faculty Publications*. 27.
https://digitalcommons.odu.edu/mae_fac_pubs/27

Original Publication Citation

Hu, N., Yang, J., Qian, S. Z., Joo, S. W., & Zheng, X. L. (2011). A cell electrofusion microfluidic device integrated with 3D thin-film microelectrode arrays. *Biomicrofluidics*, 5(3), 034121. doi:10.1063/1.3630125

A cell electrofusion microfluidic device integrated with 3D thin-film microelectrode arrays

Ning Hu,^{1,2} Jun Yang,^{1,a)} Shizhi Qian,^{2,3} Sang W. Joo,^{2,a)}
and Xiaolin Zheng¹

¹Key Laboratory of Biorheological Science and Technology, Ministry of Education,
Key Laboratory for Optoelectronic Technology and Systems, Ministry of Education,
Chongqing University, Chongqing 400030, People's Republic of China

²School of Mechanical Engineering, Yeungnam University, Gyongsan 712-749, South Korea

³Institute of Micro/Nanotechnology, Old Dominion University, Norfolk, Virginia 23529,
USA

(Received 2 June 2011; accepted 3 August 2011; published online 30 August 2011)

A microfluidic device integrated with 3D thin film microelectrode arrays wrapped around serpentine-shaped microchannel walls has been designed, fabricated and tested for cell electrofusion. Each microelectrode array has 1015 discrete microelectrodes patterned on each side wall, and the adjacent microelectrodes are separated by coplanar dielectric channel wall. The device was tested to electrofuse K562 cells under a relatively low voltage. Under an AC electric field applied between the pair of the microelectrode arrays, cells are paired at the edge of each discrete microelectrode due to the induced positive dielectrophoresis. Subsequently, electric pulse signals are sequentially applied between the microelectrode arrays to induce electroporation and electrofusion. Compared to the design with thin film microelectrode arrays deposited at the bottom of the side walls, the 3D thin film microelectrode array could induce electroporation and electrofusion under a lower voltage. The staggered electrode arrays on opposing side walls induce inhomogeneous electric field distribution, which could avoid multi-cell fusion. The alignment and pairing efficiencies of K562 cells in this device were 99% and 70.7%, respectively. The electric pulse of low voltage (~ 9 V) could induce electrofusion of these cells, and the fusion efficiency was about 43.1% of total cells loaded into the device, which is much higher than that of the convectional and most existing microfluidics-based electrofusion devices. © 2011 American Institute of Physics. [doi:[10.1063/1.3630125](https://doi.org/10.1063/1.3630125)]

I. INTRODUCTION

Cell electrofusion utilizes electric field to merge two or more cells into a hybrid in an asexual way¹. Since the hybrid integrates genetic and epigenetic information from both parent cells, it can be used for gene expression analysis,² reprogramming somatic cells,^{3,4} developing antibody, cloning mammals, and cancer immunotherapy.⁵ Compared with other approaches for cell fusion, such as virus and chemical mediated fusion method, electrofusion has been widely used due to its major advantages, including convenience in operation and observation, being free from contamination, low toxicity, and suitability for a wide range of cell types.^{6–9}

The electrofusion process can be divided in four continuous phases.^{9,10} First, a low alternating current (AC) signal (100–300 V/cm) is applied for cell alignment/pairing.⁹ Cells move toward high electric field region and are aligned to form cell pearl chains by the induced positive dielectrophoretic (DEP) force. Second, high direct current (DC) pulses (1–10 kV/cm, pulse width: 10–50 μ s) are applied to induce reversible electroporation of cytomembrane.¹¹ Third, the

^{a)}Authors to whom correspondence should be addressed. Electronic addresses: bioyangjun@cqu.edu.cn and swjoo@ynu.ac.kr.

cytomembranes at the junction of the paired cells will reconstruct, and the cytoplasm of the paired cells will exchange. Finally, the paired cells are fused into a hybrid.

Conventional electrofusion system usually consists of a fusion chamber with two parallel plate electrodes,^{9,10} which are over 1 cm apart, and a high-voltage power generator. Due to the long distance between the two plate electrodes, an expensive high-voltage power generator is required to generate sufficiently high electric field for electrofusion. In addition, the parallel electrodes induce a uniform electric field, resulting in equal probability to induce reversible electroporation and electrofusion at each cell junction within the formed cell pearl chains, which will produce undesirable multiple cell electrofusion.¹² These disadvantages limit its widespread applications.¹³

Recently, microfluidics-based cell electrofusion is obtaining more and more attention due to its low voltage, low Joule-heating effect, and precise controllability.^{11,13–26} Due to the short distance between the patterned microelectrodes, a low voltage is sufficient to generate high electric field required for electrofusion. Therefore, it eliminates the requirement for the expensive high-voltage power generator. The existing studies on microfluidics-based cell electrofusion mainly focused on improving cell pairing and fusion efficiencies. Typically, positive DEP under AC electric field is used to control cell pairing,^{14–21} and DC pulses are used for reversible electroporation and electrofusion in the microfluidic devices. Compared with the conventional electrofusion methods, the microfluidic devices have advantages of low voltage and high efficiency in cell pairing. However, the overall yield of these chips is still relatively low due to the low integration of microelectrodes into the microdevice. A 3D microelectrode structure has been integrated into a microfluidic chip and offers the possibility and potential of high throughput cell electrofusion.^{11,16} Although the cell electrofusion efficiency of paired cells at the edge of the 3D protruding microelectrodes is high, about 20% cells are trapped in the concave gaps between two adjacent protruding microelectrodes deposited on the side walls of the microchannel. These trapped cells cannot participate the cell fusion process, resulting in low electrofusion efficiency of the total cells loaded into the device. Cells coated with biotin-streptavidin improve efficiencies in cell pairing and fusion.¹³ However, this method requires modification of cells. Gel *et al.*^{18,19} recently developed a novel micro-orifice based cell electrofusion microfluidic device without using 3D microelectrodes. The micro-orifice, whose diameter is smaller than that of the cells, creates field constriction resulting in membrane breakdown occurring nowhere but in the micro-orifice. Therefore, the device has the advantages of one-to-one cell pairing and fusion. When both cells are larger than the size of the micro-orifice, the fusant will be drawn from one side of the micro-orifice to the other by pressure, which may damage cells.²⁷ The micro-orifice based device also has difficulty to fuse cells, whose nuclei are larger than the size of the micro-orifice because the nuclei are too large to pass through the orifice due to the low fluidity of nucleus. Hydrodynamic method has been used to trap and pair different types of cells in a microfluidic chip,²⁵ and to obtain high efficiency in both pairing and fusion. However, it still uses parallel plate electrodes with a large distance to induce reversible electroporation and fusion and thus has inherent disadvantages of the conventional electrofusion method. In the existing studies, both planar thin-film microelectrode^{18–21} and bulk microelectrode^{11,13,14,16} have been widely used. The planar thin film microelectrodes are deposited at the bottom edge of the side walls of the microchannel and do not cover the entire side walls. They require high voltage to achieve cell fusion compared to the bulk microelectrodes with a high aspect ratio.

In the present study, a microfluidic device with integrated 3D thin film microelectrode arrays is developed for the first time for cell electrofusion. Comparing to the existing high aspect-ratio electrodes^{11,16} containing concave gaps between two adjacent 3D protruding microelectrodes, our microchannel wall is a sandwich structure consisted with a bottom-to-top microelectrode array, a Durimide 7510 (Arch chemicals, Norwalk, CT) microchannel with 1015 discrete thin film microelectrodes deposited on each side wall, and another metal microelectrode array. Each microelectrode array also has 1015 planar thin film microelectrodes connecting the 1015 discrete microelectrodes patterned on each side wall of the microchannel to form a 3D microelectrode structure wrapped around the microchannel wall. The electrodes on the opposing side walls are staggered in position for generating nonuniform electric field on the

plane perpendicular to the side walls. Fig. 1 schematically depicts the top (Fig. 1(a)) and 3D (Fig. 1(b)) views of the microchannel and the microelectrode structure.

II. EXPERIMENTAL METHODS

A. Chip design

The electrofusion microfluidic chip consists of a serpentine-shaped microchannel integrated with 3D thin film microelectrode arrays fabricated on quartz glass substrate, and a polydimethylsiloxane (PDMS) cover. The microchannel wall is $5900\ \mu\text{m}$ in length, $240\ \mu\text{m}$ in width, and $25\ \mu\text{m}$ in height. The width of the microchannel (i.e., the distance between two adjacent opposing microchannel walls) is $80\ \mu\text{m}$. This microchannel has an inlet and an outlet, each with $2\ \text{mm}$ diameter, for sample injection and extraction. Each microelectrode array is a $0.3\ \mu\text{m}$ thickness Au thin film with 1015 microelectrodes (each $30\ \mu\text{m}$ in both width and length), which connect the microelectrodes on the side wall. Each microelectrode of $30\ \mu\text{m}$ width on

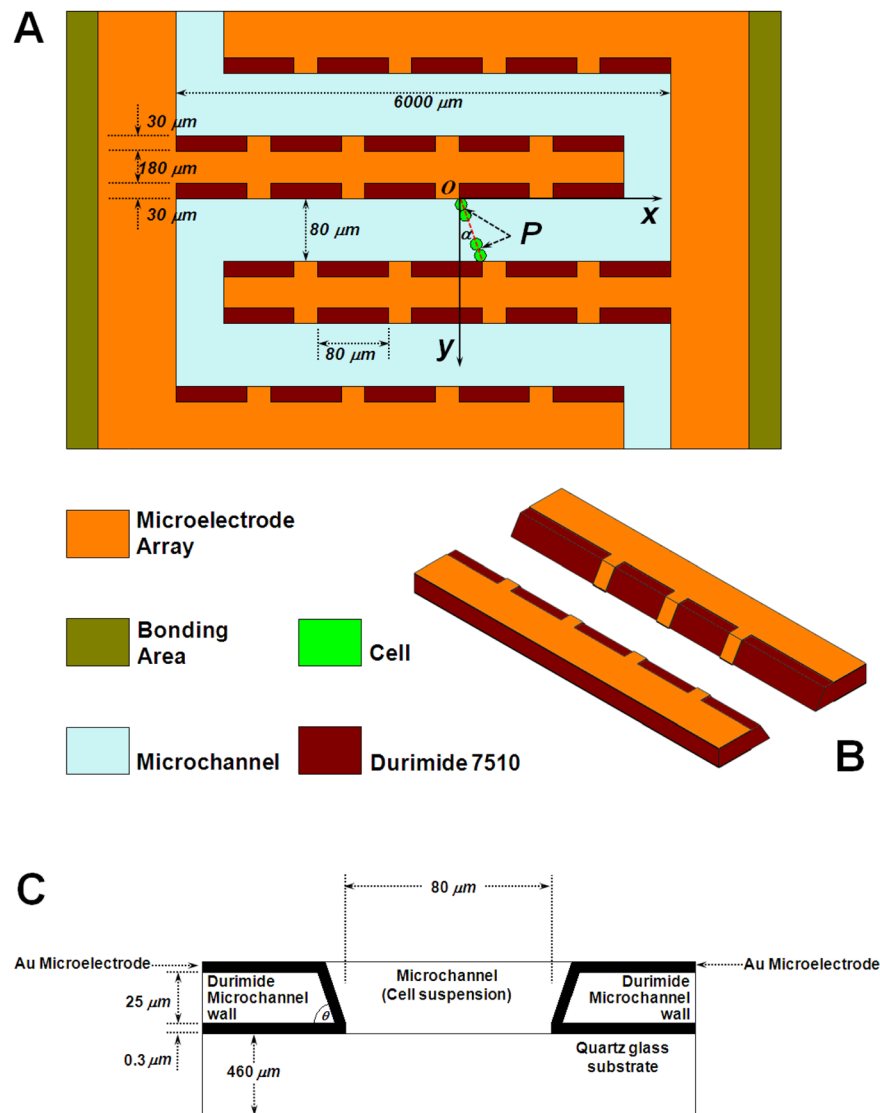


FIG. 1. Schematics of the 3D thin film microelectrode array. (a) Top view of the microchannel and the cell junction point, P. (b) Schematic view of the 3D thin film microelectrode array. (c) A cross section perpendicular to the flow direction.

the side wall covers the entire depth of the side wall and connects the corresponding microelectrodes on the top and bottom microelectrode arrays.

The overall dimensions of the chip are 22 mm (length) \times 10 mm (width) \times 0.49 mm (height), and the microelectrode array area is 6.4 mm (length) \times 10 mm (width). The total length of 20 serpentine-shaped microchannels is 120 mm.

B. Fabrication

The microchannel integrated with 3D thin film microelectrode arrays was fabricated by using the standard lithography technology, schematically shown in Fig. 2. A 460 μm thickness quartz glass was chosen as the substrate. It has a good light transmission window for observation and thus is used as a solid support for the microelectrode array structure. Au was chosen for the microelectrode array due to its good biocompatibility and electric conductivity. Before fabrication of the Au microelectrode array, a 5 nm Ti film was first sputtered on the quartz glass for a good adhesion between the Au microelectrode array and the quartz glass substrate (B). A 300 nm Au film was then magnetron sputtered on the Ti film to fabricate the bottom microelectrode array (C). A 5 μm thick AZ4620 photoresist was then coated on the Ti/Au film (D), and the bottom microelectrode array pattern was formed by photolithography (E). Subsequently, the structure of the bottom microelectrode array was formed by etching Au/Ti with KI solution (28 g KI, 20 g I_2 , 800 ml H_2O) and HF solution, followed by removing the AZ4620 resist with acetone (F). After that, a 40 μm thick Durimide 7510 layer was stacked on the pattern obtained from the previous step (G), and the pattern of the microchannel and inlet and outlet were formed by standard lithography. After formation of the microchannel structure, the unwanted Durimide 7510 was cleaned by acetone. The wafer was then put into a high temperature curing furnace at 350°C for 45 min to cure the Durimide 7510. Due to the deformation during the high temperature curing procedure of the Durimide 7510, the angle between the side

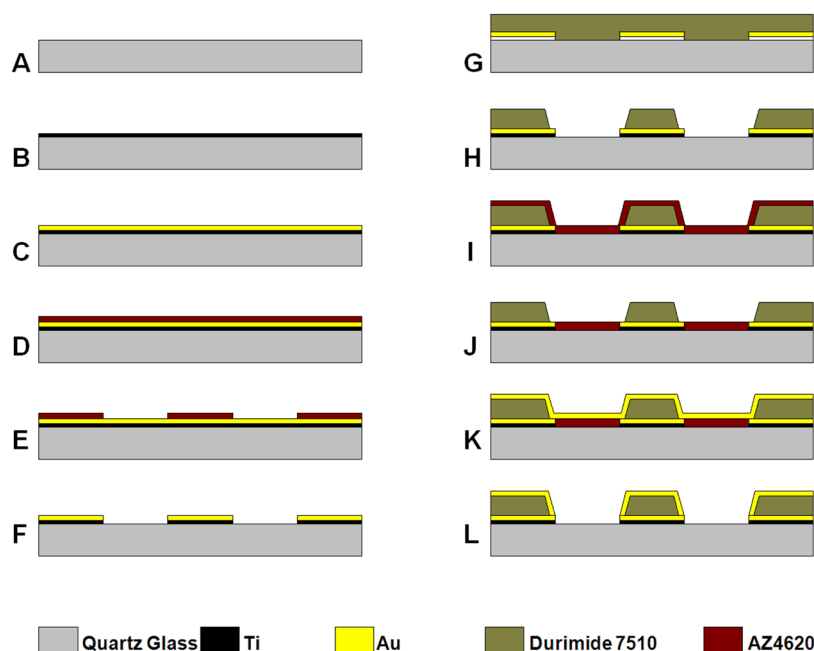


FIG. 2. The fabrication process (A \rightarrow L) of the 3D thin film microelectrode array. (A) A clean quartz glass; (B) sputter Ti film; (C) sputter Au film; (D) coat AZ4620 resist; (E) form the pattern of the bottom microelectrode array by photolithography; (F) etch the Au/Ti film; (G) stack Durimide 7510 film; (H) form the microchannel by lithography and high temperature curing; (I) coat AZ4620 photoresist as the sacrifice layer; (J) remove AZ4620 resist except the bottom of the microchannel by photolithography followed by washing with acetone; (K) sputter Au film; (L) remove the unwanted Au film by removing the sacrifice AZ4620 resist.

wall and bottom plane is about 65° , and the thickness of the Durimide 7510 changes to $25\text{ }\mu\text{m}$ (H). AZ4620 resist was then deposited again (I) and was removed except the bottom of the microchannel after photolithography (J). Finally, a 300 nm Au film was first magnetron sputtered (K), and the unwanted Au film was washed with the AZ4620 resist by acetone (L). The 3D microelectrode structure wrapping around the microchannel wall is formed. Fig. 3(a) shows a photo of the fabricated device, and the scanning electron microscopy image of the 3D thin film microelectrode array and the microchannel is shown in Fig. 3(b).

After fabrication of the microchannel integrated with 3D thin film microelectrode arrays, it was covered by a PDMS slide, which was fabricated by the standard soft lithography technique. Two holes of 2 mm in diameter connecting the inlet and outlet on the Durimide 7510 microchannel layer are punched for sample injection and extraction. Two tubes of 2 mm in diameter are plugged into the holes and fixed by PDMS. The PDMS slide was then bonded to the substrate after plasma treatment. The microchip is placed and fixed on a glass slide, and two gold wires of $200\text{ }\mu\text{m}$ in diameter are bonded at the bonding points of the microelectrode arrays of opposing side walls.

C. Cell culture

Human leukemia K-562 cells were used to test the developed device for cell electrofusion. The K562 cells were obtained from the Children's Hospital of Chongqing Medical University. These cells were maintained in a standard cell culture incubator ($5\%\text{ CO}_2$, $95\%\text{ humidity}$, 37°C). They were cultured in Roswell Park Memorial Institute (RPMI) 1640 medium supplemented with $10\%\text{ Fetal Bovine Serum (FBS)}$ [Hyclone], and subcultured every 72 h by using Phosphate Buffered Saline (PBS) buffer. Before K562 cells were used in the experiments, they were separated from the culture medium by centrifugation at 1000 rpm for 10 min and then washed three times with hypoosmolar electrofusion buffer (Osmolality: $90 \pm 10\text{ mOsmol/kg}$, Eppendorf Co. Ltd., Germany). The sediments were suspended and adjusted in the electrofusion buffer to obtain K562 cell suspension with concentration of $8.0 \times 10^6\text{ cells/ml}$.

D. Cell electrofusion experiments

The cell electrofusion experimental platform consists of a home-made signal generator, an image recorder, an Olympus BX51M microscope (Olympus Optical Co. Ltd., Japan), a syringe micropump (Gene&I Scientific Ltd., China) for sample loading and extraction, and the fabricated microfluidic device integrated with 3D thin film microelectrode arrays. The signal generator can generate AC (V_{p-p} : $0\text{--}20\text{ V}$, frequency: $0\text{--}3\text{ MHz}$), DC pulse ($0\text{--}50\text{ V}$, duration: $10\text{--}990\text{ }\mu\text{s}$, pulse number: $1\text{--}99$, and interval: $100\text{--}9990\text{ ms}$), damping quasi-sine signal (V_{p-p} : $0\text{--}20\text{ V}$, frequency: $0\text{--}3\text{ MHz}$, attenuation rate: $-50\%/min$) for cell alignment, reversible electroporation, and cytomembrane reconstruction/cytoplasm exchange, respectively.

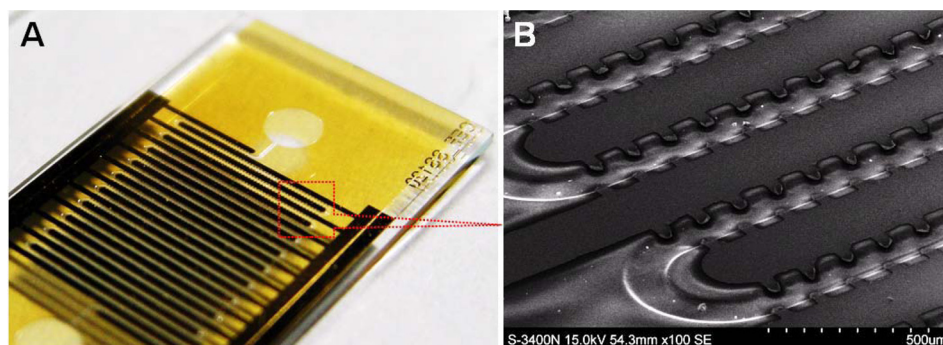


FIG. 3. Photo of the microfluidic device. (a) Unpackaged chip with a dimension of 22 mm (length) \times 10 mm (width) \times 0.49 mm (depth); (b) Scanning electron microscopy image of the microchannel in $100\times$.

The microchannel was first rinsed and washed by fresh electrofusion buffer for 30 s. Subsequently, the cell suspension was loaded into the microchannel by a syringe micropump with flow rate of 10 $\mu\text{l/h}$ until it filled the entire microchannel. The pump was then turned off, and an alignment signal (V_{p-p} : 3 V, frequency: 1 MHz) was imposed between the 3D microelectrode arrays on the opposing side walls of the microchannel. Driven by the induced positive DEP force, cells inside the microchannel are attracted toward the microelectrodes on the side walls and aligned as pairs with a high efficiency. After the cell alignment, the electroporation signal (DC electric pulses, 9 V, duration: 50 μs , interval of two pulses: 1 s, and the number of pulses: 4) was applied to induce reversible cell electroporation. Subsequently, a damping quasi-sine signal (2 V, frequency: 1 MHz, attenuation rate: $-50\%/min$, time: 300 s) was applied to generate a positive DEP force on the cells for stable contact of cells, cell membrane reconstruction, and cytoplasm exchange of the paired cells. The entire cell electrofusion process takes about 6 min. After that, hybrid cells and un-fused cells were pumped out and collected by a tube. The microchannel was washed for 30 s by using fresh electrofusion buffer and prepared for next experiment.

The experiments are repeated for 12 times. The efficiencies of the cell pairing and electrofusion of this device are characterized by $E_p = 2 \times \text{paired cells}/\text{total cells}$ and $E_f = 2 \times \text{fused cells}/\text{total cells}$, which are ensemble average of the 12 experiments obtained from the microscopic observation.^{25,28} In each experiment, about 200 cells are observed within the microscope visual field.

III. RESULTS AND DISCUSSION

A. The effect of the 3D thin film microelectrode

To illustrate the advantages of the integrated 3D thin film microelectrode over the existing planar thin film microelectrodes patterned only at the bottom edge of the side walls, we simulated the electric field distributions of both structures using the commercial finite element package, COMSOL MULTIPHYSICS (www.comsol.com). Fig. 4 schematically depicts both structures, the thin-film microelectrode structure (model 1) and the 3D thin-film microelectrode structure (model 2). Since different fabrication process can form side walls with different slopes, the effect of the angle between the side wall and the bottom substrate, θ , was also considered in both models. Microchannel made of photosensitive Durimide 7510 with $\theta = 65^\circ$ is formed by using the lithography and high temperature curing technology, while side walls with $\theta = 90^\circ$ is fabricated by dry etching technology. The following parameters were used in the 3D simulations: the conductivity of the cell suspension buffer is 1.2×10^{-4} S/m (Eppendorf Co. Ltd.), the conductivities of the Au film, quartz glass, and Durimide 7510 are 4.56×10^7 S/m, 1×10^{-12} S/m, and 1×10^{-14} S/m, respectively.²⁹ The Ti film is neglected because its thickness is only 5 nm, and its conductivity is very close to that of Au. The electrostatics is governed by the Laplace equation in the three-dimensional space. 9 V DC voltage is applied between the two counter microelectrode arrays with continuity in current and insulation condition, respectively, imposed as boundary conditions at the interface between two adjacent materials and at the dielectric material/air interface.

Since the electric-field gradient along the connecting line of the edges of the two counter microelectrodes (the red dashed line in Fig. 1(a)) is the strongest,¹¹ cells are always aligned along this line,²⁹ as schematically shown in Fig. 1(a). Cells settle down to the bottom of the microchannel due to a gravity, and the position of the junction, P , of the paired cells is $x = d \sin \alpha$, $y = d \cos \alpha$, and $z = d/2$, where d is the diameter of the cell. Here, α is the angle between the y -axis and the connecting line of the edges of the two opposite microelectrodes. Fig. 5 depicts the predicted y -component electric field (E_y) at the cell junction point as a function of the cell diameter. The magnitude of E_y at the cell junction from the 3D microelectrode structure (model 2) is always higher than that from the thin film microelectrode (model 1). For K562 cells of diameter of 12.0 ± 1.2 μm , the electric field strengths at the cell junction point for $\theta = 65^\circ$ and 90° in the model 1 are 60.8% and 48.9% those in the model 2, respectively. Therefore, a higher voltage is required for the thin film microelectrode array patterned at the bottom

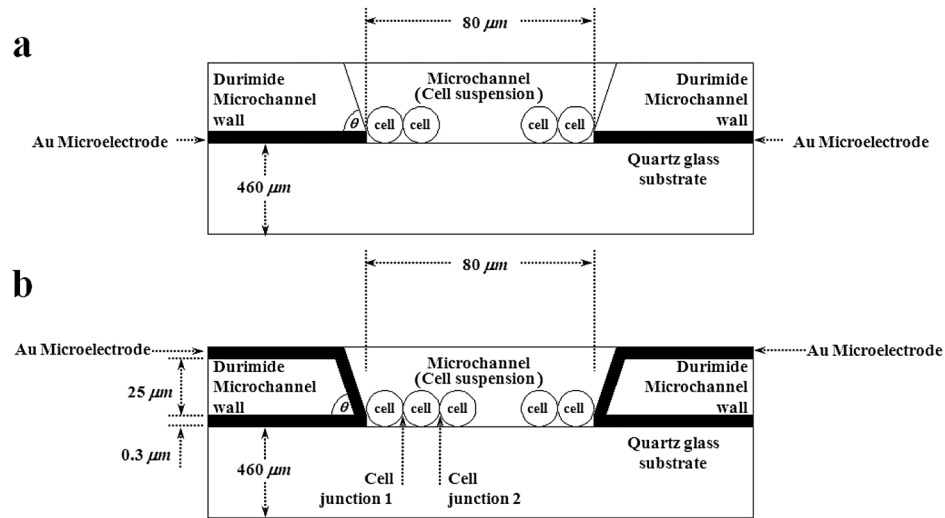


FIG. 4. Geometries of two models: (a) a planar thin film microelectrode array positioned on the bottom of the Durimide microchannel wall, (b) 3D thin film microelectrode array wrapping around the Durimide microchannel wall.

edge of the channel wall to achieve sufficiently high electric field for cell fusion. To achieve sufficient electric-field strength for reversible electroporation of K562 cells, the voltage applied to the thin film microelectrode array is almost twice that of the 3D thin film microelectrode array.

The slope of the side wall also significantly influences the electric field distribution in the microchannel. For the 3D microelectrode structure wrapped around the entire microchannel wall, the y -component electric field in the z -direction is a constant for $\theta = 90^\circ$. When θ decreases from 90° to 65° , the strength of the electric field at the cell junction point decreases 4.4%–13.2% for cell diameters ranging from $6\ \mu\text{m}$ to $20\ \mu\text{m}$, as shown in Fig. 5. For the thin film microelectrode only positioned at the bottom of the channel wall (Fig. 4(a) and model 1), the electric field strength also decreases as the angle θ decreases. For $\theta = 65^\circ$, besides the gravity, the z -component DEP force also drags cells toward the bottom wall of the microchannel,³⁰ which will accelerate the cell sedimentation. The fabrication of the microchannel with 90° side-walls requires dry etching, which can result in some remnant spots on the surface of the Durimide 7510. This will adversely affect the coating of the Au thin film on the Durimide 7510

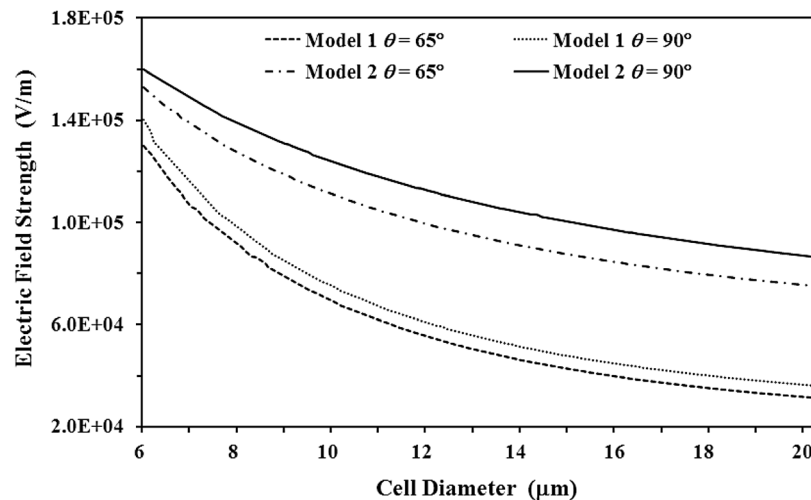


FIG. 5. The predicted y -component electric field at the cell junction point for different cell diameters.

sidewalls. Fabrication of the designed device using photosensitive Durimide 7510 by lithography and high temperature curing is much easier than the dry etching technique. In addition, the formed smooth surface and the 65° sidewalls are also helpful for later sputtering and forming Au thin film.

B. Cell alignment

In the cell-alignment experiments, an AC electric field of high strength and frequency is applied between the two 3D thin film microelectrode arrays. Since the permittivity of the cell cytoplasm, ϵ_c , is higher than that of the suspension medium, ϵ_s , cells in the microchannel will be driven by the induced positive DEP force to the high electric field region and are attached on the thin film microelectrodes deposited on the sidewalls of the microchannel. We found that most cells ($>99\%$) are successfully aligned along the connecting line between two opposite microelectrodes, shown in Fig. 1(a). In the previous 3D protruding microelectrode array, which serves as both the electrode and the entire side wall of the microchannel,^{11,16} about $22.6\% \pm 6.4\%$ cells are also aligned near the metal film in the concave regions, as shown in Fig. 6. Due to the lower electric-field strength in the gap regions, paired cells in the gap regions are not fused, and only those at the edge of the protruding electrodes are fused. In contrast, in our new design, the adjacent discrete microelectrodes on each side wall are separated by the dielectric Durimide 7510 channel wall, and they are almost co-planar. Therefore, these “dead areas” present in the previous design are filled by the dielectric Durimide 7510 and are completely eliminated in the new design. Since the gap between adjacent discrete microelectrodes is made of dielectric material, no cells are aligned and trapped in the dielectric gap, and more than 99% cells are successfully trapped at the edge of the discrete microelectrodes on both side walls, as shown in Fig. 7. About $70.7\% \pm 4.5\%$ cell pearl chains only contain two cells, and chains with one cell or more than 2 cells also occur, as shown in Fig. 7. The efficiency of forming cell-cell twins ($70.7\% \pm 4.5\%$) obtained from the new device is much higher than that ($\sim 46\%$) using the 3D protruding microelectrode array.²⁹

C. Electroporation and fusion

After cell alignment, the electroporation signal was applied to the microelectrode arrays on the opposing side walls to yield reversible electroporation on cell membranes. Due to the fluidity of the cell membrane, it is temporarily electroporated and restored spontaneously.¹⁸ Subsequently, damping quasi-sine signal was imposed for 5 min to induce a DEP force on the cell pairs for stabilizing their contact. The use of the damping quasi-sine signal prevents breakdown of the membrane of the fused cell. The cytoplasm of the paired cells were exchanged and merged with the reconstruction of membrane. Finally, most paired cells are fused into hybrids, as shown in Figs. 8 and 9. The electrofusion efficiency of all cells loaded into the device is

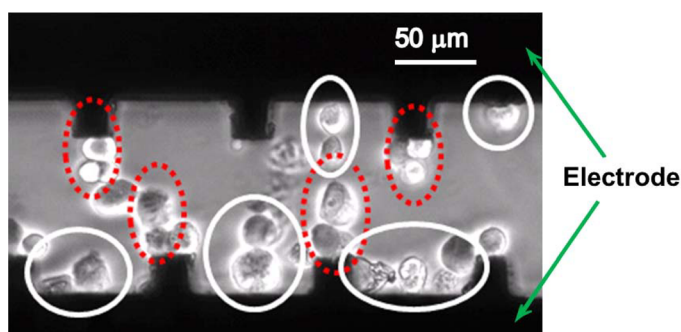


FIG. 6. Cell alignment in a microchannel with 3D protruding microelectrode array. Red dashed circles show a pair of cells aligned at the edge of the protruding microelectrodes, while white solid circles show that some cells are trapped in the gaps between two adjacent protruding microelectrodes.

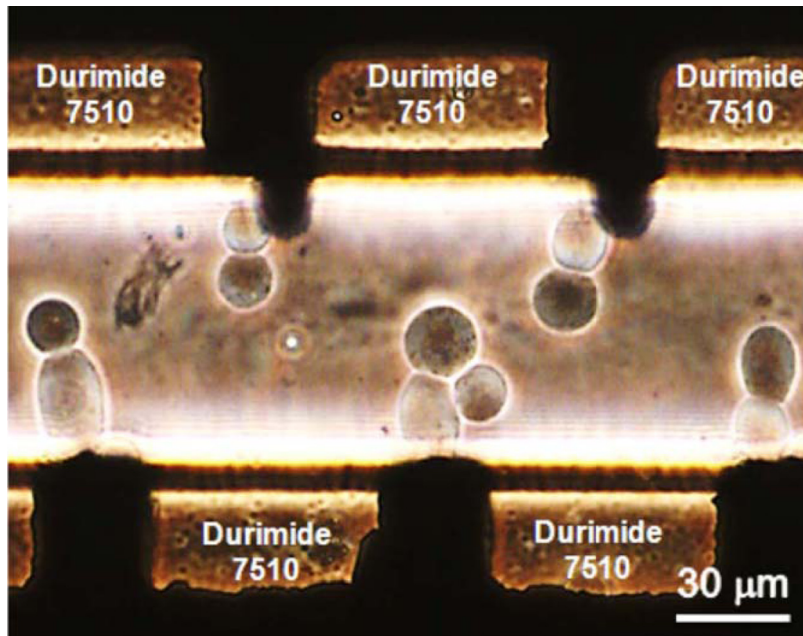


FIG. 7. Cell alignment and pairing near each microelectrode.

about $43.1\% \pm 5.8\%$, which is much higher than that ($\sim 21\%–30\%$) obtained from the device with 3D protruding microelectrode arrays.^{11,29}

Although cell pearl chains with more than two cells are possible to occur, as shown in Fig. 7, multiple cell fusion could be avoided in this device. For example, the chain with a red circle shown in Fig. 9 contains three cells, and only the first and the second cells are fused into

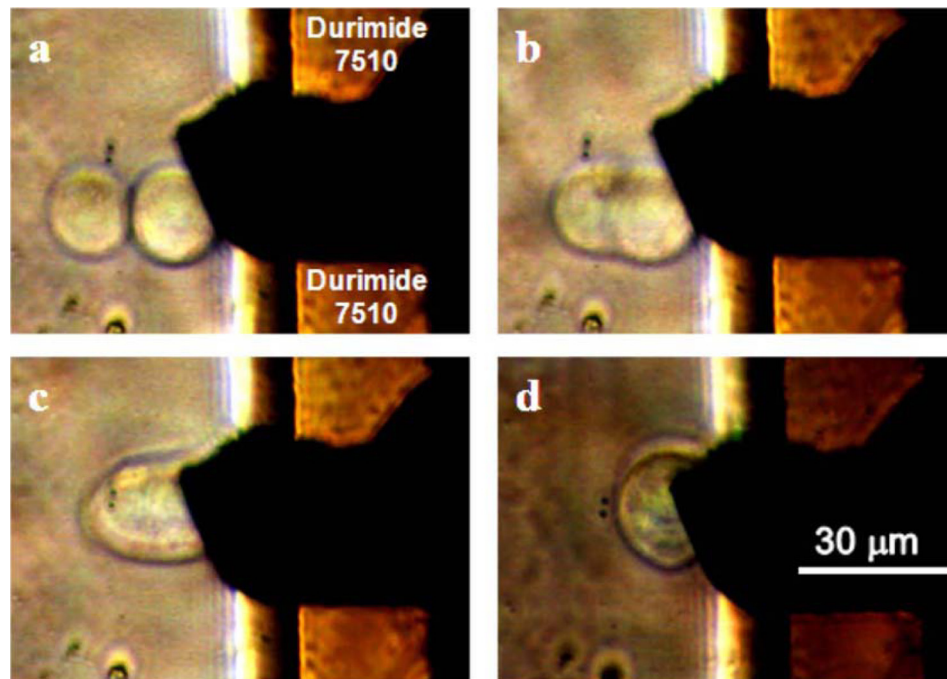


FIG. 8. The electrofusion process of K562 cells. (a) cell pairing (30 s after cell alignment signal imposed); (b) reversible electroporation at cell junction (10 s after electroporation signal imposed); (c) fusion starts (30 s after electrofusion signal imposed); (d) complete fusion (180 s after electrofusion signal imposed).

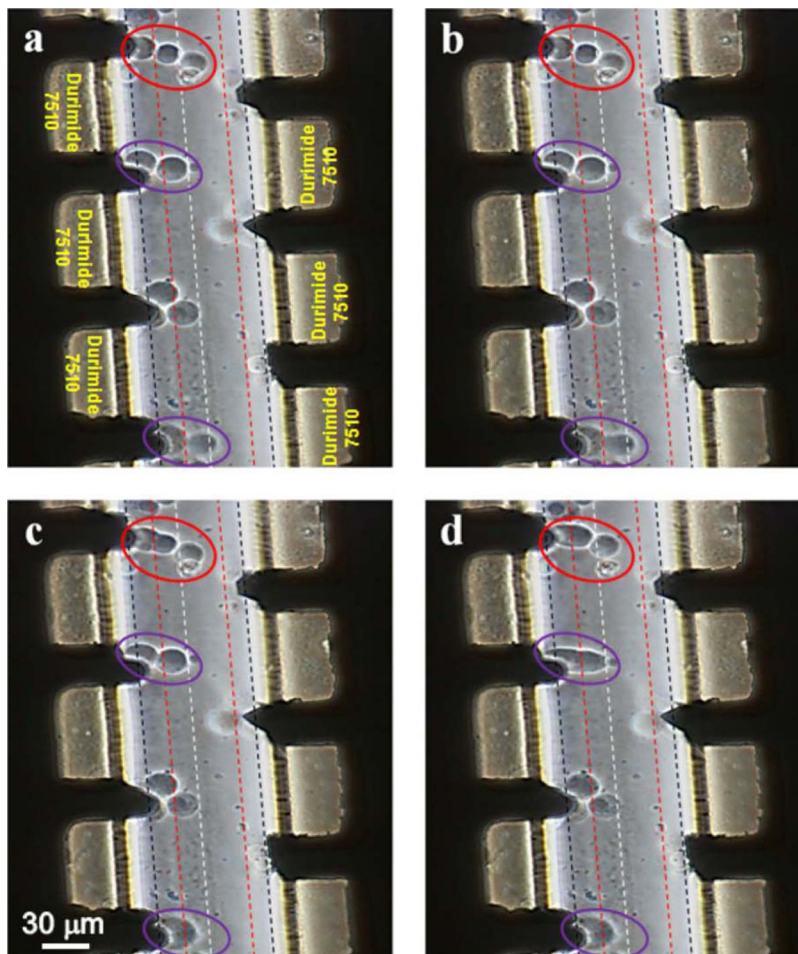


FIG. 9. The fusion process (a \rightarrow d) of two cells in the formed cell pearl chains. The purple circles are cell electrofusion between cell pairs, while the red circle shows the electrofusion occurring only at the first cell junction.

a hybrid after the application of the electroporation and fusion signals. The third cell located far away from the microelectrode did not involve the fusion of the two cells closed to the microelectrode. Fig. 4(b) schematically shows a cell pearl chain with three cells formed at the left microelectrode, and Fig. 10 depicts the predicted y-component electric field at the cell junction 1 between the first two cells (dash-dotted line) and the second cell junction between the second and third cells (solid line) as a function of the cell diameter. For the K562 cells of $12.0 \pm 1.2 \mu\text{m}$ in diameter, the difference in the electric field strength at the two junctions is more than 300 V/cm. The electric field strength at the second cell junction is much lower than that at the first cell junction and is not sufficient to form reversible electroporation and cell fusion at the second cell junction. Therefore, for a long cell chain with more than two cells, only the two cells near the microelectrode can be fused to a hybrid, and the possibility of multiple cell fusion in a long cell pearl chain is very low under appropriate control of the imposed voltages for electroporation and fusion. The choice of the electric fields for electroporation and fusion, which only allow the first cell junction to be fused, is an optimization problem. Since most cells are paired as cell-cell twins (shown in Fig. 7) and the second cell junction does not fuse under the conditions we chose (shown in Fig. 9), we rarely observed multi-cell fusion occurring in this device under the conditions we chose.

After the cell electrofusion, PBS buffer with high permittivity is introduced into the micro-channel. Subsequently, the cell alignment signal is imposed again, and negative DEP occurs due to high permittivity of the PBS buffer solution. All (hybrid and un-fused) cells are focused

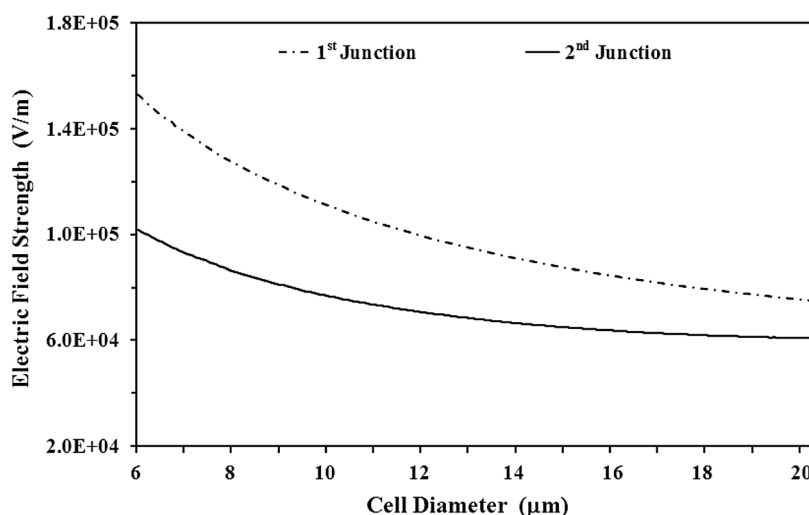


FIG. 10. The predicted y-component electric field at the first (dash-dotted line) and second (solid line) cell junctions as a function of the cell's diameter.

to the central region of the microchannel due to negative DEP and are then pumped out of the microchannel by the syringe pump.

IV. CONCLUSIONS

An integrated 3D thin film microelectrode array based cell-electrofusion microfluidic chip has been designed, fabricated, and tested with human leukemia K562 cells. There are 1015 discrete 3D thin film microelectrodes wrapped around each microchannel wall to induce more uniform electric field along the channel depth direction, which reduces the voltage for electrofusion. The adjacent microelectrodes are separated by dielectric channel wall, and they are almost co-planar, which successfully eliminated the “dead areas” occurring in the previous 3D protruding microelectrode array.^{11,16} Over 99% cells are aligned at the edge of the microelectrodes and form cell pearl chains after the application of the cell alignment signal. About 70.7% cell pearl chains only contain cell-cell twins. To avoid multiple cell fusion, the discrete microelectrodes on both side walls are staggered in position. For a long chain with more than two cells, only the two cells near the microelectrode are fused due to insufficient electric field strength at other cell junctions. The obtained results are repeatable, and the averaged fusion efficiency of total cells loaded into the device was $43.1\% \pm 5.8\%$, which is much higher than that of the traditional polyethylene glycol method (less than 5%),³¹ the traditional electrofusion methods ($\sim 12\%$),³² and most existing microfluidic devices ($\sim 21\%–30\%$).^{11,29} This new device only uses electric field to achieve cell pairing and fusion without the need of extra hydrodynamic force during the cell pairing and/or the postfusion steps. The experimental procedure is simple and efficient.

ACKNOWLEDGMENTS

This work was financially supported by the National Natural Science Foundation of China (Grant No. 30870661), the Korea Institute of Machinery & Materials (KIMM), and the World Class University Grant No. R32-2008-000-20082-0 of the Ministry of Education, Science and Technology of Korea.

¹G. Köhler and C. Milstein, *Nature (London)* **256**, 495 (1975).

²E. H. Chen and E. N. Olson, *Science* **308**, 369 (2005).

³R. A. Miller and F. H. Ruddle, *Cell* **9**, 45 (1976).

⁴M. Tada, Y. Takahama, K. Abe, N. Nakatsuji, and T. Tada, *Curr. Biol.* **11**, 1553 (2001).

⁵I. Wilmut, A. E. Schnieke, J. McWhir, A. J. Kind, and K. H. S. Campbell, *Nature (London)* **385**, 810 (1997).

- ⁶R. Jahn, T. Lang, and T. C. Sudhof, *Cell* **112**, 519 (2003).
- ⁷C. A. Cowan, J. Atienza, D. A. Melton, and K. Eggan, *Science* **309**, 1369 (2005).
- ⁸D. J. Ambrosi, B. Tanasijevic, A. Kaur, C. Obergefell, R. J. O'Neill, W. Krueger, and T. P. Rasmussen, *Stem Cells* **25**, 1104 (2007).
- ⁹U. Zimmermann and J. Vienken, *J. Membr. Biol.* **67**, 165 (1982).
- ¹⁰U. Zimmermann and P. Scheurich, *Planta* **151**, 26 (1981).
- ¹¹Y. Cao, J. Yang, Z. Q. Yin, H. Y. Luo, M. Yang, N. Hu, J. Yang, D. Q. Huo, C. J. Hou, Z. Z. Jiang, R. Q. Zhang, R. Xu, and X. L. Zheng, *Microfluid. Nanofluid.* **5**, 669 (2008).
- ¹²M. Usaj, K. Trontelj, D. Miklavcic, and M. Kanduser, *J. Membr. Biol.* **236**, 107 (2010).
- ¹³J. Wang and C. Lu, *Appl. Phys. Lett.* **89**, 234102 (2006).
- ¹⁴F. Yang, X. M. Yang, H. Jiang, P. Bulkhaits, P. Wood, W. Hrushesky, and G. R. Wang, *Biomicrofluidics* **4**, 013024 (2010).
- ¹⁵I. F. Cheng, H. C. Chang, D. Hou, and H. C. Chang, *Biomicrofluidics* **1**, 021503 (2007).
- ¹⁶G. Tresset and S. Takeuchi, *Biomed. Microdevices* **6**, 213 (2004).
- ¹⁷B. Techaumnat, K. Tsuda, O. Kurosawa, G. Murat, H. Oana, and M. Washizu, *IET Nanobiotechnol.* **2**, 93 (2008).
- ¹⁸M. Gel, S. Suzuki, Y. Kimura, O. Kurosawa, B. Techaumnat, H. Oana, and M. Washizu, *IEEE Trans. Nanobiosci.* **8**, 300 (2009).
- ¹⁹M. Gel, Y. Kimura, O. Kurosawa, H. Oana, H. Kotera, and M. Washizu, *Biomicrofluidics* **4**, 022808 (2010).
- ²⁰A. L. Clow, P. T. Gaynor, and B. J. Oback, *Biomed. Microdevices* **12**, 777 (2010).
- ²¹J. Ju, J. M. Ko, H. C. Cha, J. Y. Park, C. H. Lim, and S. H. Lee, *J. Micromech. Microeng.* **19**, 015004 (2009).
- ²²F. J. Liu, Y. Zhang, Y. M. Zheng, M. T. Zhao, Y. L. Zhang, Y. S. Wang, G. H. Wang, F. S. Quan, and Z. X. An, *Small Rum. Res.* **73**, 246 (2007).
- ²³D. T. Chiu, *Curr. Opin. Chem. Biol.* **5**, 609 (2001).
- ²⁴W. H. Tan and S. Takeuchi, *Lab Chip* **6**, 757 (2006).
- ²⁵A. M. Skelley, O. Kirak, H. Suh, R. Jaenisch, and J. Voldman, *Nat. Methods* **6**, 147 (2009).
- ²⁶P. J. Lee, P. J. Hung, R. Shaw, L. Jan, and L. P. Lee, *Appl. Phys. Lett.* **86**, 223902 (2005).
- ²⁷N. N. Ma, K. W. Koelling, and J. J. Chalmers, *Biotechnol. Bioeng.* **80**, 428 (2002).
- ²⁸A. Clow, P. Gaynor, and B. Oback, *Biomed. Microdevices* **11**, 851 (2009).
- ²⁹N. Hu, J. Yang, Z. Q. Yin, Y. Ai, S. Qian, I. B. Svir, B. Xia, J. W. Yan, W. S. Hou, and X. L. Zheng, *Electrophoresis* (2011) (in press).
- ³⁰C. Iliescu, G. Tresset, and G. L. Xu, *Biomicrofluidics* **3**, 044104 (2009).
- ³¹Q. Z. Guan, Y. H. Guo, Y. X. Wei, F. Z. Meng, and Z. X. Zhang, *Plant Cell Tissue Organ Cult.* **102**, 279 (2010).
- ³²X. Yu, P. A. McGraw, F. S. House, and J. E. Crowe, *J. Immunol. Methods* **336**, 142 (2008).